Journal of Applied Polymer Science

WILEY

Applied Polymer SCIENCE

RESEARCH ARTICLE

Multifunctional Polyvinyl Alcohol Films Incorporating *Hypericum perforatum* Essential Oil: Antibacterial Activity and Shape Memory Performance Supported by Molecular Docking

Nihan Ünlü

Department of Medical Services and Technique, Vocational School of Health Services, İstanbul Gelişim University, İstanbul, Türkiye

Correspondence: Nihan Ünlü (nunlu@gelisim.edu.tr)

Received: 23 February 2026 | **Revised:** 18 May 2026 | **Accepted:** 12 June 2026

Keywords: *Hypericum perforatum* essential oil | molecular docking | multifunctional biomaterials | polyvinyl alcohol films | shape memory polymers

ABSTRACT

The development of multifunctional antimicrobial materials represents a promising strategy to address the growing challenge of antimicrobial resistance. In this study, polyvinyl alcohol (PVA) films incorporating *Hypericum perforatum* essential oil (HPEO) at different concentrations (0.1%–0.3%) were fabricated and systematically characterized. Structural interactions were analyzed by FTIR, while optical transparency and UV-barrier performance were evaluated using UV–Vis spectroscopy. Thermal and thermomechanical behavior were examined by DSC and DMA, respectively. The incorporation of HPEO induced slight modifications in hydrogen bonding interactions and produced moderate plasticization effects without introducing additional phase transitions. Shape memory analysis revealed enhanced shape fixity (up to 98.00%) and high recovery ratios (> 95%), indicating improved temporary shape stabilization while preserving elastic recovery. Antibacterial evaluation against *Escherichia coli* ATCC 25922 demonstrated concentration-dependent inhibition, with the highest activity observed for the 0.3% formulation. To elucidate potential molecular mechanisms, bioinformatics-guided molecular docking was performed against virulence-associated proteins (1WXR, 4MEE, 3EFY, 5WIO). Docking analysis (RMSD = 0.00 Å) revealed strong multi-target binding affinities, particularly for kielcorin, mangiferin, and chlorogenic acid (up to −9.8 kcal/mol). The integration of experimental and computational findings suggests that HPEO incorporation enables the development of structurally stable, UV-protective, shape-memory active films with antibacterial functionality supported by multi-target virulence modulation.

1 | Introduction

Antimicrobial resistance (AMR), largely accelerated by the widespread and often inappropriate use of antibiotics, has become one of the most urgent global health threats. Resistant bacterial infections reduce the effectiveness of existing therapies, increase mortality rates, and impose a growing socioeconomic burden worldwide. The World Health Organization has identified AMR as a critical priority requiring the development of alternative antimicrobial strategies beyond conventional antibiotics [1].

Among clinically significant pathogens, Gram-negative bacteria such as *Escherichia coli* remain major contributors to both intestinal and extraintestinal infections. The pathogenicity of *E. coli* is closely associated with virulence determinants including adhesion mechanisms, toxin production, immune evasion, and biofilm formation, which collectively enhance

survival and persistence in host environments [2]. These challenges highlight the necessity for new antimicrobial agents that are effective, sustainable, and less prone to resistance development.

In recent years, naturally derived bioactive compounds have attracted increasing attention as promising alternatives due to their broad-spectrum antimicrobial potential and generally favorable safety profiles. Essential oils and plant secondary metabolites have been widely reported as effective antimicrobial agents, offering multi-target mechanisms that may reduce the likelihood of resistance emergence [3].

Within this context, *Hypericum perforatum* L. (St. John's Wort) has been extensively studied as a medicinal plant with a rich phytochemical composition and diverse pharmacological properties. Its bioactive constituents include hypericin, hyperforin, flavonoids, tannins, and phenolic derivatives, which are associated with antibacterial, antiviral, anti-inflammatory, and wound-healing activities [4, 5]. The therapeutic relevance of *H. perforatum* and its chemical diversity make it a strong candidate for incorporation into functional biomaterials.

However, the effective biomedical utilization of such plant-derived compounds requires suitable carrier systems that ensure stability, controlled release, and localized activity. Polymeric films have emerged as versatile platforms for antimicrobial applications, particularly in wound dressings and infection-preventive coatings. Polyvinyl alcohol (PVA) is one of the most widely used synthetic polymers in biomedical engineering due to its biocompatibility, non-toxicity, hydrophilicity, and excellent film-forming ability [6]. Furthermore, the incorporation of natural antimicrobial agents into PVA matrices has been shown to enhance biological performance while maintaining desirable mechanical integrity.

Beyond antibacterial activity, the development of multifunctional smart polymer systems is of growing interest for next-generation biomedical materials. Shape memory polymers (SMPs), which can recover their original shape after deformation under external stimuli such as temperature, provide unique opportunities for responsive wound dressings and dynamic biomedical devices [7]. Semi-crystalline polymers such as PVA are particularly promising in this regard, as their hydrogen-bonding networks and crystalline domains can support thermally triggered shape recovery behavior [8].

In parallel with experimental investigations, molecular docking has become an essential computational approach for predicting ligand–protein interactions and supporting antimicrobial mechanism analysis. Docking simulations provide valuable insight into binding affinity and potential inhibitory pathways, strengthening the rational design of bioactive materials [9, 10].

In addition to docking, bioinformatics-based analyses have emerged as powerful tools for exploring bacterial resistance mechanisms and identifying potential molecular targets involved in pathogenicity and drug susceptibility. By integrating genomic and protein-level information, bioinformatics enables the systematic screening of key bacterial genes, virulence factors, and essential enzymes that may serve as promising targets for plant-derived antimicrobial compounds. Such approaches not only enhance the mechanistic interpretation of experimental findings but also contribute to the development of more effective and targeted antibacterial strategies [11, 12]. Therefore, the combination of bioinformatics-informed insights with molecular docking offers a comprehensive framework for exploring ligand–target interactions and gaining a deeper understanding of the antibacterial potential of natural compounds.

In this study, multifunctional PVA films incorporating *Hypericum perforatum* essential oil at different concentrations (0.1%, 0.2%, and 0.3%) were successfully fabricated. The structural, optical, thermal, and mechanical characteristics of the films were systematically evaluated using Fourier transform infrared spectroscopy (FTIR), UV–Vis spectroscopy, differential scanning calorimetry (DSC), and dynamic mechanical analysis (DMA). Shape memory performance was investigated to assess the smart functional response of the materials. In addition, antibacterial activity against *E. coli* was experimentally examined, while molecular docking analysis, supported by bioinformatics-based insights, was employed to elucidate the interaction mechanisms of selected bioactive compounds with bacterial targets.

2 | Materials and Methods

2.1 | Materials

Polyvinyl alcohol (PVA) powder and glutaraldehyde solution (25 wt% in water) were purchased from Merck. The PVA used in this study had an average molecular weight in the range of 30,000–70,000 g/mol and a degree of hydrolysis of 87%–90%. *Hypericum perforatum* L. essential oil (St. John's Wort essential oil, HPEO) was obtained from Sigma-Aldrich. For antibacterial activity assays, the Gram-negative bacterial strain *Escherichia coli* (*ATCC 25922*) was used. The bacterial cultures were maintained under appropriate laboratory conditions in our microbiology facility.

2.2 | Preparation of PVA Films Incorporating *Hypericum perforatum* Essential Oil

Polyvinyl alcohol-based films were prepared using the direct incorporation method, as previously described in our earlier work [13], with slight modifications regarding the type and concentration of the essential oil incorporated into the polymer matrix.

Hypericum perforatum L. essential oil (HPEO) was incorporated into the homogeneous Polyvinyl alcohol solution at different concentrations of 0.1%, 0.2%, and 0.3% (v/v). The mixtures were stirred thoroughly to ensure uniform dispersion of the essential oil within the polymer matrix.

The resulting solutions were cast onto clean, leveled glass Petri dishes and dried under ambient conditions until complete solvent evaporation. After drying, the films were stored in a desiccator to prevent moisture uptake prior to characterization.

The prepared film samples were coded according to their essential oil content as PVA-HPEO0.1, PVA-HPEO0.2, and

PVA-HPEO0.3, while the film without essential oil (PVA) was used as the control sample.

2.3 | Fourier-Transform Infrared (FTIR) Spectroscopy

Fourier-transform infrared (FTIR) spectroscopy was employed to investigate the chemical structure of neat polyvinyl alcohol (PVA) films and PVA composite films incorporating 0.10%, 0.20%, and 0.30% (w/w) *Hypericum perforatum* essential oil. Prior to analysis, all film samples were conditioned at ambient temperature (~25°C) to ensure moisture equilibrium. FTIR spectra were recorded using a PE IR Subtech Spectrum spectrometer in the range of 4000–400 cm^{-1} at a spectral resolution of 4 cm^{-1}. For each sample, eight consecutive scans were collected and averaged, and background spectra were obtained and subtracted under identical experimental conditions. Spectra were reported in percent transmittance (%T), and film specimens were analyzed directly without further pretreatment, ensuring consistent contact within the measurement area. The spectra were examined to identify the characteristic absorption bands of PVA and to evaluate potential band shifts or intensity changes indicative of molecular interactions between the polymer matrix and essential-oil constituents.

2.4 | Optical Transmittance Analysis (UV–Vis Spectroscopy)

The optical properties of neat Polyvinyl alcohol (PVA) films and PVA composite films incorporating different concentrations of *Hypericum perforatum* essential oil were evaluated using UV–Vis spectroscopy. The light transmittance behavior of the films was examined in order to assess their transparency in the visible region as well as their potential ultraviolet (UV) barrier performance.

UV–Vis spectra were recorded over the wavelength range of 190–900 nm. Film specimens were placed directly in the sample holder, and air was used as the reference. The percentage transmittance (%T) values were obtained and comparatively analyzed to determine the influence of essential oil incorporation on the optical response of the PVA matrix.

2.5 | Thermal Characterization (Differential Scanning Calorimetry, DSC)

The thermal behavior of neat PVA and essential oil–incorporated PVA films was investigated by differential scanning calorimetry (DSC). Measurements were performed under a nitrogen atmosphere to minimize oxidative effects during heating.

Approximately 5–10 mg of each film sample was sealed in standard aluminum pans, while an empty pan was used as the reference. The samples were heated from −40°C to 100°C at a constant rate of 10°C min^{-1}, and the thermal response was continuously recorded.

The glass transition temperature (T_g) was determined from the baseline shift observed in the DSC thermograms. The effect of essential oil addition on the thermal response and molecular mobility of the polymer matrix was evaluated through comparison with neat PVA films.

2.6 | Thermomechanical Properties (Dynamic Mechanical Analysis, DMA)

The thermomechanical and viscoelastic properties of neat PVA films and *Hypericum perforatum* essential oil–loaded PVA composite films were analyzed using dynamic mechanical analysis (DMA). The measurements were carried out to evaluate the temperature-dependent deformation and viscoelastic response of the prepared film samples.

Rectangular film specimens were mounted in tensile mode, and the temperature was gradually increased according to the selected heating program. During the analysis, strain (%) was recorded as a function of temperature to monitor the structural response of the films under thermal conditions.

The resulting thermomechanical curves provided insight into the influence of essential oil incorporation on the deformation characteristics and overall stability of the PVA matrix. All measurements were carried out under identical experimental parameters to ensure reliable comparison between neat and composite film formulations.

2.7 | Shape Memory Performance Test

The shape memory behavior of the Polyvinyl alcohol–HPEO films was evaluated using a cyclic bending test, as described in our previous work [14]. Briefly, specimens (1 × 5 cm) were folded at 40°C, fixed by cooling to 5°C, and reheated to monitor shape recovery. The bending angles measured during the test (θ_{max}, θ_f, and θ_r) are schematically illustrated in Figure 1. The shape fixity (R_f) and recovery (R_r) ratios were calculated using Equations (1) and (2).

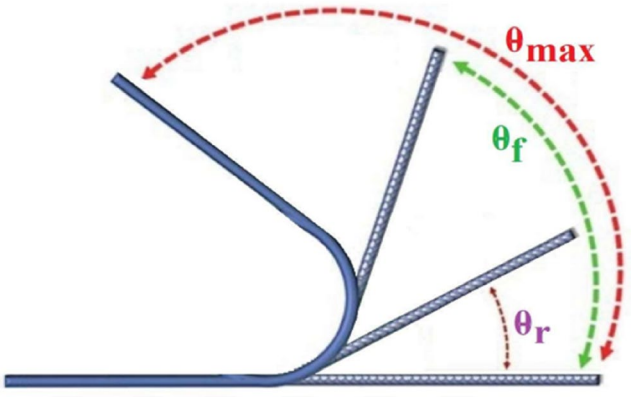

FIGURE 1 | Schematic illustration of the angles measured during the shape memory test [14]. [Color figure can be viewed at wileyonlinelibrary.com]

$$R_f = \frac{\theta_f}{\theta_{max}} \times 100 \quad (1)$$

$$R_r = \frac{\theta_f - \theta_r}{\theta_f} \times 100 \quad (2)$$

2.8 | Antibacterial Activity Evaluation

The antibacterial activity of the prepared PVA–HPEO film samples against *Escherichia coli* ATCC 25922 was determined using the agar well-diffusion method [15]. Pure PVA film was used as the negative control. As a positive control for *E. coli* ATCC 25922, amoxicillin–clavulanate (AMC, 20/10 μg/mL) was employed.

The bacterial strain was grown in LB broth for 16 h. Subsequently, *E. coli* was cultured for 16 h at 37°C on Müller–Hinton agar (MHA). The density of the bacterial suspension was adjusted to the 0.5 McFarland standard (1.5×10^8 CFU/mL) by dilution with Müller–Hinton broth (MHB) at a 1:100 ratio, in accordance with CLSI guidelines [16].

Following standardization, 100 μL of the bacterial suspension was uniformly spread onto MHA Petri dishes using a sterile spreader. Wells with a diameter of 6.0 mm were then aseptically created in the agar using sterile pipette tips. Subsequently, 100 μL of the prepared samples containing *Hypericum perforatum* essential oil at concentrations of 0.1%, 0.2%, and 0.3% were carefully transferred into the wells.

The plates were incubated at 37°C for 24 h, after which the diameters of the inhibition zones were measured in millimeters. Each experimental trial was repeated three times.

2.9 | Bioinformatics Analysis

The virulence-associated proteins of *Escherichia coli* and the corresponding amino acid sequences encoded by the selected virulence genes were retrieved from the NCBI Gene database (https://www.ncbi.nlm.nih.gov/gene/) and the Protein Data Bank (PDB). All databases were accessed on August 04, 2025.

Information regarding the conserved domains of the virulence proteins was obtained using the NCBI Conserved Domain Database (CDD) (https://www.ncbi.nlm.nih.gov/guide/domains-structures/), accessed on August 04, 2025.

The predicted subcellular localization of the virulence proteins was determined using the online server DeepLocPro-1.0 (https://services.healthtech.dtu.dk/services/DeepLocPro-1.0/), accessed on August 04, 2025.

2.10 | Molecular Docking Analysis

The three-dimensional structures of *Escherichia coli* virulence-associated target proteins were retrieved from the RCSB Protein Data Bank (PDB). The selected protein structures included PDB IDs 1WXR, 4MEE, 3EFY, and 5WIO, which were chosen due to their relevance in bacterial pathogenicity and virulence-related mechanisms.

Prior to docking simulations, protein preparation was performed using AutoDock's protein preparation tools. This optimization process involved the removal of crystallographic water molecules and the correction of structural parameters to ensure suitability for molecular interaction analysis. The prepared protein structures were subsequently used as receptors in the docking experiments.

The ligand molecules investigated in this study were bioactive phytochemical constituents of *Hypericum perforatum*, selected based on their reported antibacterial and pharmacological potential. Ligand structures, including hyperforin (PubChem CID: 516569100), adhyperforin (PubChem CID: 505548769), hypericin (PubChem CID: 3663), mangiferin (PubChem CID: 5281647), norathyriol (PubChem CID: 5281656), kielcorin (PubChem CID: 13834128), as well as several phenolic acids such as p-coumaric acid (PubChem CID: 637542), chlorogenic acid (PubChem CID: 1794427), caffeic acid (PubChem CID: 689043), vanillic acid (PubChem CID: 8468), 4-hydroxybenzoic acid (PubChem CID: 135), and ferulic acid (PubChem CID: 445858), were obtained from the NCBI PubChem database (https://www.ncbi.nlm.nih.gov/).

All ligand structures were downloaded and processed for docking analysis. The molecular files were converted into the appropriate docking format (PDBQT), and ligand optimization was carried out using the PyRx virtual screening tool (version 0.8), enabling the generation of atomic coordinates and energy-minimized conformations.

The prepared receptor proteins and optimized ligand structures were then employed in molecular docking simulations to evaluate binding affinities and explore potential interaction mechanisms between *H. perforatum* phytochemicals and *E. coli* virulence-related targets.

3 | Results and Discussion

3.1 | Structural Analysis (FTIR)

The FTIR transmittance spectra of neat PVA and PVA films incorporated with *Hypericum perforatum* essential oil (HPEO) at concentrations of 0.10%, 0.20%, and 0.30% (w/w) are presented in Figure 2. The main absorption bands and their tentative assignments are summarized in Table 1. All samples exhibit the characteristic vibrational features of PVA, while gradual spectral variations are observed upon essential-oil incorporation, indicating molecular-level interactions between the polymer chains and the bioactive constituents of the oil.

The broad band located in the range of 3200–3500 cm^{-1} is attributed to O–H stretching vibrations associated with extensive intra- and intermolecular hydrogen bonding within the PVA network [17]. With increasing HPEO content, this band shows a slight shift toward lower wavenumbers, suggesting enhanced hydrogen-bonding interactions between the hydroxyl groups of PVA and polar functional groups present in the essential oil.

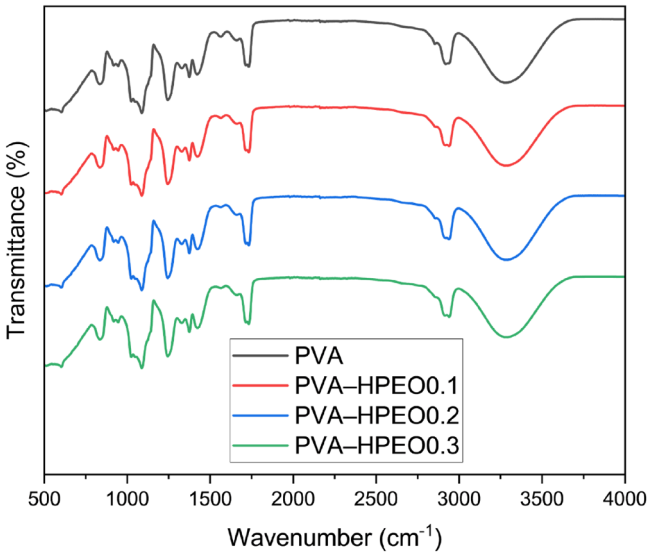

FIGURE 2 | FTIR transmittance spectra of neat Polyvinyl alcohol (PVA) and PVA composite films incorporated with *Hypericum perforatum* essential oil (HPEO) at concentrations of 0.10%, 0.20%, and 0.30% (w/w). [Color figure can be viewed at wileyonlinelibrary.com]

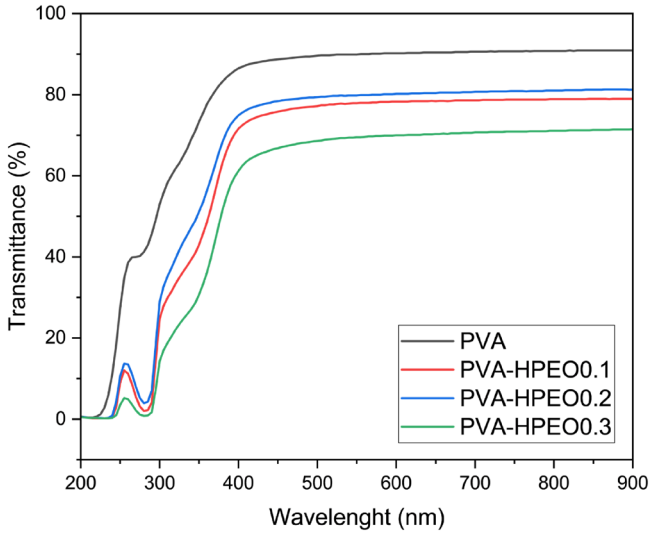

FIGURE 3 | UV–Vis transmittance spectra of neat poly(vinyl alcohol) (PVA) and PVA composite films incorporated with *Hypericum perforatum* essential oil (HPEO) at concentrations of 0.10%, 0.20%, and 0.30% (w/w). [Color figure can be viewed at wileyonlinelibrary.com]

TABLE 1 | Main FTIR absorption bands and tentative assignments for neat PVA and HPEO-loaded PVA films.

Wavenumber (cm^{-1})	Assignment	Interpretation
3200–3500	O—H stretching	Hydrogen bonding interactions (PVA–PVA/ PVA–HPEO)
2940–2850	C—H stretching ($—CH_2—$)	Vibrations of the PVA polymer backbone
~1730	C═O stretching	Residual acetate groups in partially hydrolyzed PVA
1420–1370	CH_2 bending	Changes in chain conformation and packing
1260–1020	C—O/C—O—C stretching	Contributions from oxygenated terpenes and phenolics in HPEO
840–850	C—H rocking vibration	Skeletal vibrations related to semicrystalline PVA domains

Similar behavior has been reported for PVA-based composite films containing natural additives [18, 19].

The absorption bands observed at 2940–2850 cm^{-1} correspond to C—H stretching vibrations of the $—CH_2—$ groups along the PVA backbone [17]. In the essential-oil-loaded films, a modest increase in intensity in this region may arise from additional aliphatic contributions originating from terpenoid components of the oil [20]. The absence of pronounced peak shifts suggests that these interactions remain primarily physical rather than involving chemical modification of the polymer chains.

A weak band near 1730 cm^{-1}, attributed to residual acetate groups in partially hydrolyzed PVA, remains essentially unchanged after essential-oil incorporation, indicating limited involvement of carbonyl functionalities in the interaction mechanism [17, 18]. Minor variations in this region may result from overlapping absorptions of carbonyl-containing constituents within the essential oil [20].

Further evidence for the incorporation of HPEO is observed in the fingerprint region (1500–800 cm^{-1}). Oil-containing films display subtle shoulders and additional bands, particularly in the 1260–1020 cm^{-1} range, which are associated with C—O and C—O—C stretching vibrations characteristic of oxygenated terpenes and phenolic compounds [20]. These spectral features, which are weak or absent in neat PVA, confirm the successful dispersion of essential-oil constituents within the polymer matrix.

Importantly, no new absorption bands indicative of covalent bond formation were detected. Therefore, the observed spectral changes are mainly attributed to non-covalent interactions, such as hydrogen bonding and physical entrapment, consistent with previous FTIR studies on PVA films containing functional bioactive additives [18, 19].

3.2 | Optical Properties (UV–Vis)

Figure 3 presents the UV–Vis transmittance spectra (200–900 nm) of neat polyvinyl alcohol (PVA) and PVA composite films incorporated with *Hypericum perforatum* essential oil (HPEO) at concentrations of 0.10%, 0.20%, and 0.30% (w/w). All samples exhibit a wavelength-dependent increase in transmittance, with

a pronounced rise near the UV–visible boundary followed by a relatively stable plateau across the visible region.

The neat PVA film displayed the highest optical transparency, reaching a high transmittance level throughout the visible range. This behavior is consistent with the well-established optical clarity of solution-cast PVA films reported in the literature [21].

Upon incorporation of HPEO, a gradual reduction in visible-light transmittance was observed, which became more pronounced with increasing essential-oil content. While the films containing 0.10%–0.20% HPEO retained considerable transparency, the 0.30% formulation exhibited a stronger decrease, indicating that higher oil loadings reduce optical clarity. Nevertheless, the composite films maintained appreciable transmittance, which may remain advantageous for applications requiring partial transparency, such as active packaging materials.

In the ultraviolet region, all films exhibited markedly lower transmittance compared with the visible region, suggesting an inherent UV-blocking capability. Importantly, the addition of HPEO further suppressed UV transmittance, supporting the role of plant-derived compounds as effective UV-absorbing additives. Such enhancement is generally attributed to the presence of chromophoric phytochemicals, including hypericin-related constituents in *H. perforatum*, which contribute to absorption in the UV and near-UV ranges [22, 23].

The observed decrease in transmittance following essential-oil incorporation can be explained by a combination of increased absorption from UV-active components and enhanced light scattering arising from microstructural heterogeneity within the polymer matrix. Previous studies on essential-oil-loaded polymer films have reported that dispersed oil domains may scatter incident light, thereby reducing overall transmission, particularly at higher oil concentrations [24].

From an application perspective, these results indicate that the optical response of PVA films can be effectively tuned through HPEO loading, providing a balance between visible transparency and improved UV-shielding performance. Such tunable properties are particularly relevant for the development of functional films designed to protect light-sensitive products from UV exposure [25].

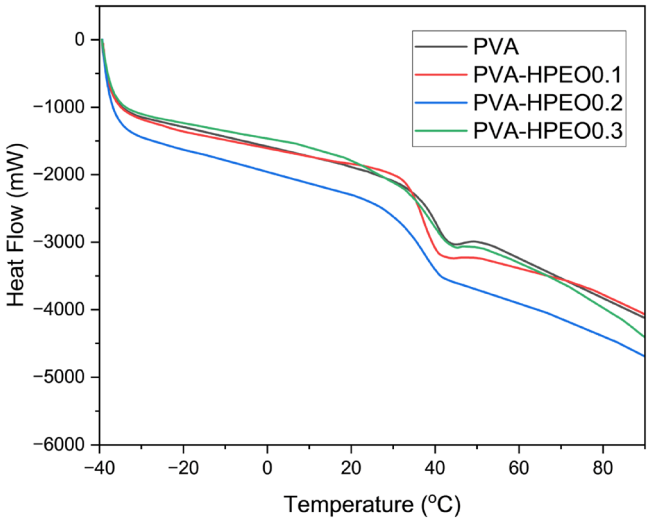

FIGURE 4 | DSC thermograms of neat polyvinyl alcohol and *Hypericum perforatum* essential oil–incorporated polyvinyl alcohol films at different oil concentrations (0.1–0.3 wt%). [Color figure can be viewed at wileyonlinelibrary.com]

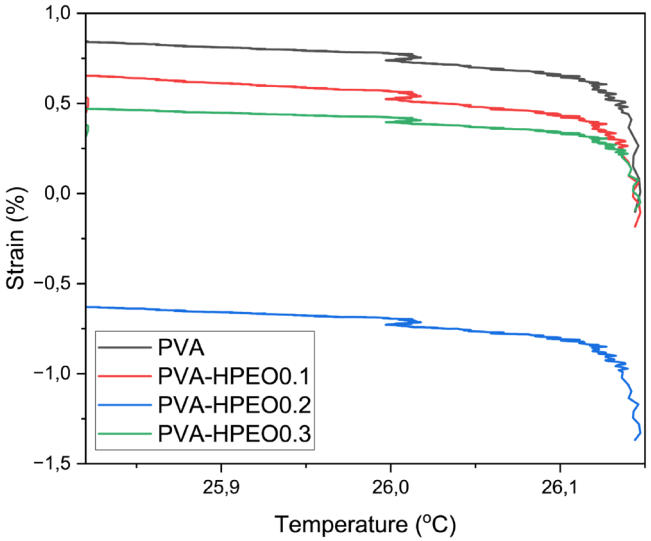

FIGURE 5 | Temperature-dependent strain response obtained from dynamic mechanical analysis (DMA) of neat Polyvinyl alcohol (PVA) and *Hypericum perforatum* essential oil (HPEO)-incorporated PVA films. [Color figure can be viewed at wileyonlinelibrary.com]

3.3 | Thermal Properties (DSC)

Figure 4 presents the DSC thermograms of neat polyvinyl alcohol and *Hypericum perforatum* essential oil–incorporated films recorded during the first heating scan. All samples exhibit a broad thermal event in the low-temperature region (≈30°C–55°C). Such low-temperature features are typical for hydrated polyvinyl alcohol systems and are commonly associated with the thermal response of sorbed/bound water (including non-freezing and freezing-bound fractions) and concurrent relaxation processes in the amorphous domains, which can appear as broad endothermic behavior in DSC. This moisture-related behavior in polyvinyl alcohol has been demonstrated by DSC-based studies focusing specifically on bound/sorbed water states in polyvinyl alcohol matrices [26, 27]. Moreover, the overlap between moisture-related events and structural relaxations is especially expected in the first heating run when residual water has not yet been fully removed or redistributed [27].

A subtle baseline shift corresponding to the glass transition of the amorphous phase was detected within 37°C–40°C. The neat polyvinyl alcohol film exhibited $T_g = 40.4$°C, while essential oil incorporation produced slightly reduced T_g values at lower loadings (37.0°C and 37.4°C for 0.1% and 0.2%, respectively), followed by a moderate increase at 0.3% (39.2°C). The initial T_g reduction is consistent with a plasticization effect of low-molecular-weight additives, which increase segmental mobility by reducing

TABLE 2 | Shape fixity (R_f) and shape recovery (R_r) ratios of neat PVA and HPEO-incorporated films over five thermomechanical cycles with statistical parameters.

	PVA		PVA-HPEO0.1		PVA-HPEO0.2		PVA-HPEO0.3	
Number of cycles	R_f (%)	R_r (%)	R_f (%)	R_r (%)	R_f (%)	R_r (%)	R_f (%)	R_r (%)
1	94.45	97.06	97.22	97.14	98.33	98.31	98.89	97.75
2	91.67	96.97	97.22	97.14	97.78	98.30	98.89	97.19
3	88.89	93.75	97.22	94.29	97.78	97.16	97.78	96.02
4	88.89	96.88	97.22	94.29	96.67	95.98	97.22	96.00
5	88.89	96.88	95.56	94.19	97.22	95.43	97.22	96.00
Average	90.56	96.31	96.89	95.41	97.56	97.04	98.00	96.59
Standard deviation	2.49	1.43	0.74	1.58	0.63	1.32	0.84	0.83
Standard error	1.11	0.64	0.33	0.71	0.28	0.59	0.38	0.37

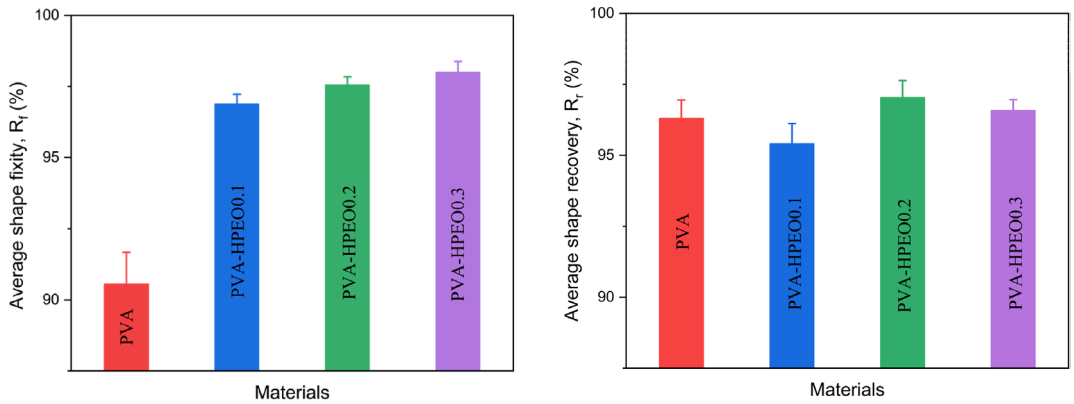

FIGURE 6 | Average shape fixity (R_f) and shape recovery (R_r) ratios of all prepared films with standard deviation error bars. [Color figure can be viewed at wileyonlinelibrary.com]

TABLE 3 | Inhibition zone diameters (mm) of polyvinyl alcohol–HPEO films against *Escherichia coli ATCC* 25922.

Treatments	Inhibition zone (mm) on *E. coli*
PVA-HPEO0.1	11
PVA-HPEO0.2	12
PVA-HPEO0.3	12.3
PVA	0
AMC[a]	20

[a]AMC: amoxicillin-clavulanate (20/10 μg/mL).

effective intermolecular interactions; such plasticizer-driven T_g depression is widely documented for polymeric film systems [28, 29]. At higher loading, the partial recovery of T_g may reflect stronger secondary interactions and/or reduced free-volume effects within the amorphous phase, yielding a slightly more constrained network.

Importantly, T_g values reported for polyvinyl alcohol films can vary substantially because they depend on polymer grade (degree of hydrolysis and molecular weight), thermal history, crystallinity, and moisture content. For example, film studies using different polyvinyl alcohol types and DSC protocols report T_g values spanning roughly the 40°C–55°C range, highlighting the sensitivity of T_g to formulation and structure [30]. In the present work, because DSC was performed as a single heating scan, residual moisture is expected to shift the apparent T_g downward, consistent with the well-established plasticizing influence of sorbed water in polyvinyl alcohol systems [27].

No melting endotherm was detected up to 100°C for either neat or composite films. This is expected because polyvinyl alcohol melting typically occurs at much higher temperatures (commonly around ~200°C and above), and clear melting peaks near ~229°C are routinely observed in DSC for polyvinyl alcohol and its plasticized composites under appropriate scan ranges [31]. Overall, the DSC results indicate that, within the investigated temperature window, the thermal behavior of the prepared films is dominated by moisture-related relaxation phenomena and the glass transition of the amorphous phase, while *Hypericum perforatum* essential oil produces only modest T_g shifts without introducing additional low-temperature phase transitions.

3.4 | Thermomechanical Properties (DMA)

The thermomechanical behavior of neat Polyvinyl alcohol and HPEO-incorporated films was evaluated by dynamic mechanical analysis. Figure 5 presents the temperature-dependent strain response of the samples, reflecting their deformation behavior under thermal loading.

Neat Polyvinyl alcohol exhibited the lowest strain values throughout the analyzed temperature interval, indicating higher resistance

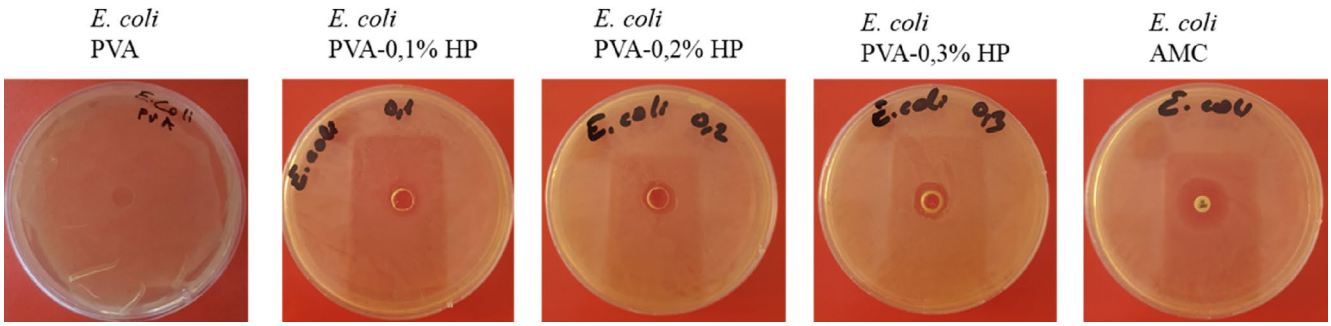

FIGURE 7 | Representative inhibition zones of Polyvinyl alcohol–HPEO films against *Escherichia coli* ATCC 25922. [Color figure can be viewed at wileyonlinelibrary.com]

TABLE 4 | Structural and functional features of selected virulence-associated proteins in *Escherichia coli*.

Bacteria	Protein ID	UniProtKB ID	Protein names	CD	Proteins (aa) lengths from UniProtKB	SL
E. coli	1WXR	O88093	Hemoglobin-binding protease hbp autotransporter	53–803; 966–1377; 828–1076	1337	EC
	4MEE	Q03155	Autotransporter adhesin AIDA-I	1–1286	1286	EC
	3EFY	Q7WRZ5	Cif (Cell cycle inhibiting factor)	105–215	282	EC
	5WIO	Q17U16	Conjugal transfer protein, TraE	1–232	232	CM

Abbreviations: CD: conserved domain; CM: cytoplasmic membrane; EC: extracellular; SL: sub-cellular location.

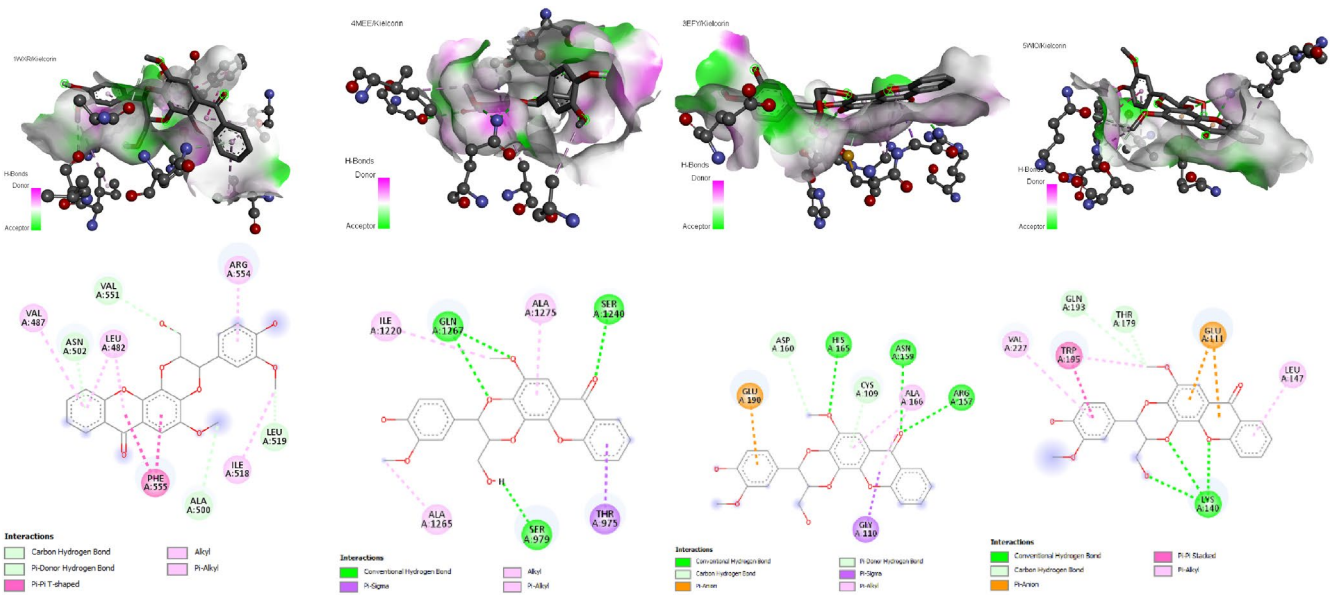

FIGURE 8 | 2D and 3D representation of the interaction between the amino acids in the binding region of the 1WXR, 4MEE, 3EFY, and 5WIO target macromolecules and the ligand kielcorin. [Color figure can be viewed at wileyonlinelibrary.com]

TABLE 5 | Docking results for 1WXR.

Protein–Ligand	Interaction type	Interacting amino acid	Binding energy/ΔG (kcal/mol)
1WXR/Hyperforin	Conventional Hydrogen Bond	ALA558	−7.0
	Alkyl	ALA558	
	Pi-Alkyl	TYR480, PHE555, TYR560, PHE698	
1WXR/Adhyperforin	Alkyl	ALA558, ALA697	−6.7
	Pi-Alkyl	PHE555, PHE698	
1WXR/P-Coumaric Acid	Pi-Sigma	LEU632	−5.6
	Pi-Donor Hydrogen Bond	SER637	
1WXR/Chlorogenic Acid	Conventional Hydrogen Bond	PHE638, SER639, PRO635, GLN634	−7.0
	Carbon Hydrogen Bond	SER637	
	Unfavorable Donor-Donor	GLN634	
	Pi-Sigma	LEU632	
	Pi-Donor Hydrogen Bond	SER637, HIS612	
1WXR/Caffeic Acid	Conventional Hydrogen Bond	ASP642	−5.6
	Pi-Donor Hydrogen Bond	SER637	
	Pi-Sigma	LEU632	
1WXR/Vanillic Acid	Conventional Hydrogen Bond	HIS612	−5.3
	Pi-Donor Hydrogen Bond	SER637	
	Pi-Sigma	LEU632	
1WXR/4-Hydroxybenzoic acid	Conventional Hydrogen Bond	HIS612, ASP642, GLN634	−5.1
	Pi-Donor Hydrogen Bond	SER637	
	Pi-Sigma	LEU632	
1WXR/Ferulic Acid	Conventional Hydrogen Bond	ASP642	−5.7
	Pi-Donor Hydrogen Bond	SER637	
	Pi-Sigma	LEU632	
	Alkyl	LEU632	
1WXR/Kielcorin	Carbon Hydrogen Bond	LEU519, VAL551, ALA500	−7.5
	Pi-Donor Hydrogen Bond	ASN502	
	Pi-Pi T-shaped	PHE555	
	Alkyl	ILE518	
	Pi-Alkyl	LEU482, VAL487, ARG554	
1WXR/Norathyriol	Conventional Hydrogen Bond	GLN634	−7.0
	Pi-Donor Hydrogen Bond	SER637	
	Pi-Alkyl	LEU632	
	Pi-Sigma	LEU632	
	Pi-Pi T-shaped	HIS612	

(Continues)

TABLE 5 | (Continued)

Protein–Ligand	Interaction type	Interacting amino acid	Binding energy/ΔG (kcal/mol)
1WXR/Mangiferin	Carbon Hydrogen Bond	HIS612, SER637, GLN634	−7.0
	Unfavorable Donor-Donor	THR633	
	Pi-Donor Hydrogen Bond	SER637	
	Pi-Sigma	LEU632	
	Pi-Pi T-shaped	HIS612	
1WXR/Hypericin	Pi-Alkyl	TRP492, TYR506, TYR526	−4.2

TABLE 6 | Docking results for 4MEE.

Protein–Ligand	Interaction type	Interacting amino acid	Binding energy/ΔG (kcal/mol)
4MEE/Hyperforin	Alkyl	ALA1100, LEU1051	−6.4
	Pi-Alkyl	PHE1049, TRP1088	
	Conventional Hydrogen Bond	THR1102	
	Pi-Sigma	PHE1049, TRP1088	
4MEE/Adhyperforin	Pi-Alkyl	TRP1088	−6.5
	Pi-Sigma	PHE1049, TRP1088	
	Alkyl	ALA1132	
4MEE/P-Coumaric Acid	Unfavorable Donor-Donor	GLN1243	−6.0
	Conventional Hydrogen Bond	THR972, THR975, ASN1274, SER1238	
4MEE/Chlorogenic Acid	Pi-Donor Hydrogen Bond	ASN1222	−9.2
	Conventional Hydrogen Bond	THR975, ASN1186, HIS1224, SER1014, SER1238	
4MEE/Caffeic Acid	Pi-Donor Hydrogen Bond	TYR1214	−6.7
	Conventional Hydrogen Bond	ARG1008, LYS1247, SER1277, LEU985	
	Pi-Anion	GLU987	
4MEE/Vanillic Acid	Carbon Hydrogen Bond	ARG1194, TYR1089	−6.1
	Alkyl	LYS989	
	Pi-Alkyl	TYR1089	
	Conventional Hydrogen Bond	SER1196, LYS1198, ASN986	
	Unfavorable Donor-Donor	ASN1094	
4MEE/4-Hydroxybenzoic acid	Conventional Hydrogen Bond	ASN1137, LYS1198	−6.0
	Unfavorable Donor-Donor	ASN1094	
4MEE/Ferulic Acid	Conventional Hydrogen Bond	THR972, SER1238, SER1240, GLN1243, ALA971, THR975, ASN1274	−6.5
	Carbon Hydrogen Bond	GLN1243	

(Continues)

TABLE 6 | (Continued)

Protein–Ligand	Interaction type	Interacting amino acid	Binding energy/ΔG (kcal/mol)
4MEE/Kielcorin	Pi-Sigma	THR975	−9.8
	Alkyl	ALA1265, ILE1220	
	Pi-Alkyl	ALA1275	
	Conventional Hydrogen Bond	SER1240, GLN1267, SER979	
4MEE/Norathyriol	Van der Waals	—	−8.7
	Conventional Hydrogen Bond	ASN1222, SER1238, SER1014, THR972	
	Unfavorable Donor-Donor	GLN1243	
	Pi-Donor Hydrogen Bond	SER1240	
	Pi-Sigma	THR975	
	Amide-Pi Stacked	SER1015, GLY1016	
4MEE/Mangiferin	Conventional Hydrogen Bond	GLN1188, SER1240, GLN1267, SER1277, SER979, SER1238	−9.6
	Carbon Hydrogen Bond	GLN1267	
	Pi-Alkyl	ALA1275	
	Unfavorable Donor-Donor	GLN1029	
	Pi-Donor Hydrogen Bond	SER979, SER1240	
4MEE/Hypericin	Pi-Alkyl	TRP1154	−4.5

to thermally induced deformation. This behavior is attributed to the strong intermolecular hydrogen bonding interactions between hydroxyl groups of adjacent PVA chains, which promote physical crosslinking and semicrystalline domain formation. Such intermolecular interactions are well known to enhance the mechanical rigidity and dimensional stability of PVA-based materials [32].

As temperature increased, a gradual rise in strain was observed for all samples, corresponding to enhanced molecular mobility and softening of the amorphous regions. This thermally activated deformation is characteristic of semicrystalline Polyvinyl alcohol systems, where chain relaxation occurs progressively with increasing temperature.

Incorporation of *Hypericum perforatum* essential oil resulted in higher strain values compared to neat PVA, particularly at 0.2 and 0.3 wt% loadings. This trend suggests a plasticization effect induced by the essential oil components. Low-molecular-weight oil constituents can partially disrupt hydrogen bonding interactions between polymer chains, increase free volume, and enhance segmental mobility. Similar plasticizing effects have been reported for essential oil–containing polysaccharide and PVA-based films [33].

At elevated temperatures, the increase in deformation became more pronounced in the composite films. This behavior may be associated with reduced cohesive forces within the polymer network and microstructural heterogeneity induced by the incorporation of low-molecular-weight essential oil components. In various studies, the addition of essential oils to polymeric matrices has been reported to weaken intermolecular interactions, disturb chain packing, and consequently reduce mechanical resistance, particularly at elevated temperatures [33, 34]. Such effects are generally attributed to partial disruption of hydrogen bonding and increased free volume within the polymer network.

Overall, the results indicate that neat polyvinyl alcohol provides superior thermomechanical stability, whereas HPEO incorporation enhances flexibility and deformation capacity under thermal stress. Therefore, essential oil concentration can be considered an effective parameter for tailoring the balance between rigidity and flexibility depending on the targeted application.

3.5 | Shape Memory Performance

The shape memory performance of the synthesized PVA and *Hypericum perforatum* essential oil (HPEO)-incorporated composite films was evaluated using the shape fixity (R_f) and shape recovery (R_r) ratios calculated from Equations (1) and (2). The average R_f and R_r values obtained over five consecutive thermomechanical cycles, together with the corresponding standard deviation and standard error values, are presented in Table 2 and Figure 6. These statistical parameters provide insight into the dispersion and reproducibility of the measurements. The relatively low standard deviation and standard error values obtained for all sample groups indicate a narrow data distribution

TABLE 7 | Docking results for 3EFY.

Protein–Ligand	Interaction type	Interacting amino acid	Binding energy/ΔG (kcal/mol)
3EFY/Hyperforin	Alkyl	PRO172, MET202, LEU207, ILE116, LEU119, ILE270	−7.1
	Pi-Alkyl	PHE120, PHE182	
	Conventional Hydrogen Bond	TYR184	
	Pi-Sigma	TYR184	
3EFY/Adhyperforin	Pi-Alkyl	PHE120, TYR184	−7.1
	Conventional Hydrogen Bond	TYR184	
	Alkyl	LEU207, ILE270, ILE274	
3EFY/P-Coumaric Acid	Unfavorable Aceptor-Aceptor	GLN142	−5.4
	Conventional Hydrogen Bond	ASP256, ASN257, PHE258	
	Pi-Sigma	LEU138	
3EFY/Chlorogenic Acid	Unfavorable Donor-Donor	PHE258	−6.7
	Carbon Hydrogen Bond	HIS255	
	Conventional Hydrogen Bond	GLU139, GLN142, SER220, HIS255, ASP256, ASN257, SER223	
3EFY/Caffeic Acid	Pi-Pi Stacked	HIS255	−5.3
	Conventional Hydrogen Bond	ASP256, LYS254, ASN257	
	Unfavorable Donor-Donor	ASN257	
	Pi-Alkyl	LEU138	
	Pi-Sigma	SER223	
3EFY/Vanillic Acid	Carbon Hydrogen Bond	SER137, ASP256	−5.7
	Unfavorable Aceptor-Aceptor	SER223	
	Pi-Alkyl	LEU138	
	Conventional Hydrogen Bond	LEU138, HIS255, ASN257, PHE258	
3EFY/4-Hydroxybenzoic acid	Conventional Hydrogen Bond	ASN257, PHE258	−4.9
	Pi-Alkyl	LEU138	
	Unfavorable Donor-Donor	ASN257, ASP256	
3EFY/Ferulic Acid	Conventional Hydrogen Bond	ASN257, PHE258	−5.5
	Pi-Sigma	LEU138	
	Carbon Hydrogen Bond	SER220, SER223, GLN224	
	Unfavorable Donor-Donor	ASP256	
3EFY/Kielcorin	Pi-Sigma	GLY110	−7.4
	Pi-Donor Hydrogen Bond	CYS109	
	Pi-Alkyl	ALA166	
	Pi-Anion	GLU190	
	Carbon Hydrogen Bond	ASP160	
	Conventional Hydrogen Bond	ARG157, ASN159, HIS165	

(Continues)

TABLE 7 | (Continued)

Protein–Ligand	Interaction type	Interacting amino acid	Binding energy/ΔG (kcal/mol)
3EFY/Norathyriol	Conventional Hydrogen Bond	SER146, ASN176	−6.6
	Carbon Hydrogen Bond	SER146	
	Pi-Anion	ASP213	
	Pi-Sulfur	CYS216	
	Pi-Alkyl	LEU145	
3EFY/Mangiferin	Conventional Hydrogen Bond	SER220, PHE258, SER223	−6.6
	Carbon Hydrogen Bond	SER223	
	Pi-Alkyl	LEU138	
	Unfavorable Donor-Donor	ASN257, PHE258	
	Pi-Donor Hydrogen Bond	GLN142	
3EFY/Hypericin	Pi-Alkyl	ILE116, LEU119, ILE274	−4.6
	Alkyl	PHE120, TRY184	

and good cyclic stability, suggesting that the programmed and recovered shapes were consistently maintained during repeated testing [14, 35, 36].

For neat polyvinyl alcohol, the average R_f and R_r values were calculated as 90.56% and 96.31%, respectively. Upon incorporation of HPEO, both parameters showed a marked improvement. The average R_f values increased to 96.89%, 97.56%, and 98.00% for PVA-HPEO0.1, PVA-HPEO0.2, and PVA-HPEO0.3 films, respectively, while the corresponding R_r values were 95.41%, 97.04%, and 96.59%. The increase in R_f suggests a more efficient temporary shape fixation capability in the presence of HPEO, whereas the high R_r values indicate that sufficient elastic restoring forces were preserved within the polymer network to enable effective recovery.

The highest shape fixity ratio was observed for the 0.3% HPEO-containing film, whereas the 0.2% formulation exhibited the highest shape recovery ratio. This behavior may reflect a balance between enhanced intermolecular interactions and maintained chain mobility. At moderate HPEO content, improved physical interactions—likely mediated by hydrogen bonding between hydroxyl groups of polyvinyl alcohol and functional groups present in the essential oil—may reinforce the temporary network structure without excessively restricting segmental motion required for recovery. Such behavior is consistent with the mechanistic framework of thermally triggered shape memory polymers, where the interplay between network elasticity and switching segment mobility governs fixation and recovery efficiency [36, 37].

Cycle-dependent analysis revealed a slight decreasing trend in both R_f and R_r values with increasing cycle number for all samples. Such behavior is commonly reported in physically crosslinked shape memory polymers and is generally attributed to partial chain relaxation, minor structural rearrangements, and gradual redistribution of physical interactions under repeated thermomechanical loading [7, 35, 38]. Nevertheless, the reductions observed here were limited, indicating that the network structure remained largely intact over 5 cycles.

Overall, the incorporation of HPEO appears to modify the intermolecular interaction landscape within the polyvinyl alcohol matrix, resulting in improved fixation efficiency while maintaining high recovery performance and cyclic stability. The findings demonstrate that essential oil incorporation influences not only the magnitude of shape memory ratios but also the stability of the thermomechanical response during repeated programming–recovery cycles.

3.6 | Antibacterial Evuluation

The antibacterial activity of polyvinyl alcohol–HPEO composite films against *Escherichia coli* ATCC 25922 was evaluated, and the inhibition zone diameters are presented in Table 3. Representative inhibition halos are shown in Figure 7.

Neat Polyvinyl alcohol exhibited no inhibitory effect against *E. coli*, confirming the absence of intrinsic antibacterial activity. In contrast, all HPEO-incorporated films produced visible inhibition zones, indicating that antimicrobial functionality was imparted by the incorporation of *Hypericum perforatum* essential oil. A slight increase in inhibition zone diameter was observed with increasing essential oil concentration. The PVA-HPEO0.3 film demonstrated the highest activity, with an inhibition zone of 12.3 mm.

Although the antibacterial effect remained lower than that of the positive control (amoxicillin–clavulanate, 20 mm), the results confirm a concentration-dependent inhibitory response against *E. coli*. The formation of inhibition halos suggests diffusion of bioactive compounds from the film matrix into the surrounding medium.

TABLE 8 | Docking results for 5WIO.

Protein–Ligand	Interaction type	Interacting amino acid	Binding energy/ΔG (kcal/mol)
5WIO/Hyperforin	Alkyl	LYS140, LEU147, VAL227	−7.7
	Pi-Alkyl	TYR113, PHE141, TRP195	
	Conventional Hydrogen Bond	LYS140, THR157, GLU111	
	Pi-Sigma	TRP195	
5WIO/Adhyperforin	Pi-Alkyl	PHE177, TRP195	−7.0
	Pi-Sigma	TRP195	
	Conventional Hydrogen Bond	THR157	
	Unfavorable Donor-Donor	GLN193	
	Alkyl	ARG181	
5WIO/P-Coumaric Acid	Conventional Hydrogen Bond	VAL227	−5.6
	Pi-Anion	GLU111	
	Pi-Pi Stacked	TRP195	
	Pi-Alkyl	VAL227	
5WIO/Chlorogenic Acid	Conventional Hydrogen Bond	LYS140, THR157, THR179	−7.2
5WIO/Caffeic Acid	Pi-Anion	GLU111	−5.5
	Conventional Hydrogen Bond	VAL227, THR179	
	Pi-Alkyl	VAL227	
	Pi-Pi Stacked	TRP195	
5WIO/Vanillic Acid	Conventional Hydrogen Bond	THR179, TRP195, GLU111	−5.1
	Pi-Anion	GLU111	
	Pi-Alkyl	TRP195, VAL227	
	Pi-Pi Stacked	TRP195	
5WIO/4-Hydroxybenzoic acid	Conventional Hydrogen Bond	THR179, TRP195, GLU111	−5.2
	Pi-Anion	GLU111	
	Pi-Pi Stacked	TRP195	
	Pi-Alkyl	VAL227	
5WIO/Ferulic Acid	Conventional Hydrogen Bond	THR179, TRP195, GLU111	−5.5
	Carbon Hydrogen Bond	GLU111	
	Pi-Pi T-shaped	TRP195	
	Pi-Alkyl	TYR225, VAL227	
5WIO/Kielcorin	Pi-Anion	GLU111	−7.8
	Pi-Pi Stacked	TRP195	
	Carbon Hydrogen Bond	THR179, GLN193	
	Pi-Alkyl	TRP195, LEU147, VAL227	
	Conventional Hydrogen Bond	LYS140	

(Continues)

TABLE 8 | (Continued)

Protein–Ligand	Interaction type	Interacting amino acid	Binding energy/ΔG (kcal/mol)
5WIO/Norathyriol	Conventional Hydrogen Bond	THR157, THR179, TRP195	−6.3
	Pi-Anion	GLU111	
	Pi-Pi Stacked	TRP195	
	Pi-Alkyl	VAL227	
5WIO/Mangiferin	Conventional Hydrogen Bond	LYS140, THR157, VAL227, GLU111	−7.0
	Pi-Anion	GLU111	
5WIO/Hypericin	Alkyl	LYS100, VAL164, LEU166	−3.7

Foodborne diseases represent a significant global public health concern with implications for food safety, economic stability, and social development [39]. Since *E. coli* is a well-recognized foodborne pathogen, the demonstrated antibacterial performance of the Polyvinyl alcohol–HPEO films suggests their potential application as active packaging materials aimed at reducing microbial contamination risks in food systems.

3.7 | Bioinformatic Analysis

Microbial pathogens possess specialized molecules, known as virulence factors, that enable colonization, survival, and infection within the host [40]. These factors include toxins, surface-associated adhesins, secretion-associated proteins, and nutrient acquisition systems that collectively contribute to pathogenicity [41].

Iron acquisition is a critical determinant of bacterial survival under host-imposed iron limitation. The hemoglobin-binding protease Hbp (PDB ID: 1WXR) plays a functional role in extracting heme from hemoglobin and supplying it to the bacterium, thereby supporting growth during infection [42].

Autotransporter adhesins such as AIDA-I (PDB ID: 4MEE) mediate bacterial attachment to host epithelial cells and are associated with autoaggregation and biofilm formation, which enhance bacterial persistence and colonization efficiency [43, 44].

The cycle-inhibiting factor Cif (PDB ID: 3EFY), identified in pathogenic *Escherichia coli* strains, is known to induce host cell cycle arrest and cytopathic effects [45].

TraE (PDB ID: 5WIO), a conjugative transfer protein associated with the cytoplasmic membrane, participates in pilus assembly and contributes to bacterial adhesion and horizontal gene transfer processes [46].

The structural characteristics, conserved domains (CD), and sequence features of these virulence-associated proteins are summarized in Table 4. The predicted subcellular localization analysis indicated that proteins 1WXR, 4MEE, and 3EFY are extracellular, whereas 5WIO is associated with the cytoplasmic membrane. Subcellular localization is closely linked to protein accessibility and biological function, and such information is important for evaluating potential ligand–protein interaction feasibility [47].

Based on their established roles in virulence and predicted structural accessibility, the selected proteins were considered suitable molecular targets for docking analysis. The docking results revealed that the interacting amino acid residues identified in Figure 8 are located within or in close proximity to conserved regions previously characterized for each protein (Tables 5–8). The alignment between conserved domain mapping and ligand interaction sites suggests that binding occurs in structurally relevant regions associated with functional activity. Although molecular docking provides theoretical insight into potential ligand–protein interactions, the observed consistency between bioinformatic characterization and docking findings strengthens the rationale for targeting these virulence-associated proteins.

3.8 | Molecular Docking Analysis

Docking simulations were conducted to assess the interaction potential of *Hypericum perforatum* phytochemicals against *Escherichia coli* virulence-associated proteins (1WXR, 4MEE, 3EFY, 5WIO). Only binding poses with RMSD = 0.00 Å were considered to ensure structural reliability and selection of the top-ranked energetically stable conformations [48, 49].

Binding energies ranged from −4.2 to −9.8 kcal/mol (Tables 5–8). Among all compounds, kielcorin exhibited the strongest and most consistent affinities, reaching −9.8 kcal/mol against 4MEE and maintaining favorable binding (≈−7.4 to −7.8 kcal/mol) across the remaining targets. Mangiferin and chlorogenic acid also demonstrated stable multi-target interaction profiles.

Interaction mapping revealed that high-affinity ligand predominantly formed conventional hydrogen bonds, π–π stacking, π–anion, and hydrophobic π-alkyl contacts (Figure 8). The cooperative contribution of hydrogen bonding (specificity) and π/hydrophobic interactions (stabilization) is consistent with established structure-based docking principles [50].

Notably, 4MEE displayed the most favorable binding energies overall, suggesting a binding cavity particularly compatible with polyphenolic scaffolds. The repeated involvement of conserved residues across different targets supports structural complementarity between aromatic hydroxyl-rich ligands and virulence-associated functional domains.

Binding energies below −7.0 kcal/mol are commonly reported in virtual screening studies as indicative of potentially favorable ligand–target interactions [50]. The convergence of low docking scores and RMSD = 0.00 Å poses strengthens the robustness of the predicted complexes.

Collectively, the consistent multi-target affinity—particularly for kielcorin, mangiferin, and chlorogenic acid—suggests that *Hypericum perforatum* phytochemicals may exert antibacterial activity through simultaneous modulation of virulence-related proteins.

4 | Conclusion

This study demonstrates that incorporation of *Hypericum perforatum* essential oil enables the development of multifunctional polyvinyl alcohol films combining structural stability, tunable optical behavior, enhanced shape memory performance, and concentration-dependent antibacterial activity. Essential oil addition modulated intermolecular interactions within the polymer matrix without inducing detrimental thermal instability, while simultaneously improving shape fixation efficiency. The observed inhibition against *Escherichia coli* was further supported by bioinformatics-guided molecular docking, which revealed stable multi-target interactions of key phytochemicals with virulence-associated proteins. The convergence of experimental and computational findings highlights the potential of HPEO-incorporated polyvinyl alcohol films as promising candidates for active biomedical or antimicrobial packaging applications. Future studies focusing on release kinetics and in vivo validation will further clarify their translational potential.

Author Contributions

Nihan Ünlü: writing – original draft, writing – review and editing, project administration, resources, data curation, conceptualization, visualization, validation, methodology, software, formal analysis.

Acknowledgments

I would like to thank Prof. Ali Durmuş (Istanbul University-Cerrahpaşa) for his support in providing access to analytical instrumentation and technical guidance, and Dr. Arzu Özgen (Istanbul Gelişim University) for her assistance with the antibacterial experiments and bioinformatics analyses.

Funding

The author has nothing to report.

Conflicts of Interest

The author declares no conflicts of interest.

Data Availability Statement

The data that support the findings of this study are available from the corresponding author upon reasonable request.

References

1. World Health Organization, *Global Antimicrobial Resistance Surveillance System (GLASS) Report: Early Implementation 2020* (World Health Organization, 2020).

2. J. B. Kaper, J. P. Nataro, and H. L. T. Mobley, "Pathogenic *Escherichia coli*," *Nature Reviews Microbiology* 2, no. 2 (2004): 123–140, https://doi.org/10.1038/nrmicro818.

3. F. Nazzaro, F. Fratianni, L. de Martino, R. Coppola, and V. de Feo, "Effect of Essential Oils on Pathogenic Bacteria," *Pharmaceuticals* 6, no. 12 (2013): 1451–1474, https://doi.org/10.3390/ph6121451.

4. J. Barnes, L. A. Anderson, and J. D. Phillipson, "St John's Wort (*Hypericum perforatum* L.): A Review of Its Chemistry, Pharmacology and Clinical Properties," *Journal of Pharmacy and Pharmacology* 53, no. 5 (2001): 583–600, https://doi.org/10.1211/0022357011775910.

5. S. L. Crockett and N. K. Robson, "Taxonomy and Chemotaxonomy of the Genus Hypericum," *Medicinal and Aromatic Plant Science and Biotechnology* 5, no. Special Issue 1 (2011): 1–13.

6. C. M. Hassan and N. A. Peppas, "Structure and Applications of Poly(Vinyl Alcohol) Hydrogels Produced by Conventional Crosslinking or by Freezing/Thawing Methods," in *Advances in Polymer Science* (Springer Berlin Heidelberg, 2000), 37–65, https://doi.org/10.1007/3-540-46414-x_2.

7. A. Lendlein and S. Kelch, "Shape-Memory Polymers," *Angewandte Chemie International Edition* 41, no. 12 (2002): 2034, https://doi.org/10.1002/1521-3773(20020617)41:12<2034::aid-anie2034>3.0.co;2-m.

8. T. Xie, "Tunable Polymer Multi-Shape Memory Effect," *Nature* 464, no. 7286 (2010): 267–270, https://doi.org/10.1038/nature08863.

9. G. M. Morris and M. Lim-Wilby, "Molecular Docking," in *Methods in Molecular Biology* (Humana Press, 2008), 365–382, https://doi.org/10.1007/978-1-59745-177-2_19.

10. N. S. Pagadala, K. Syed, and J. Tuszynski, "Software for Molecular Docking: A Review," *Biophysical Reviews* 9, no. 2 (2017): 91–102, https://doi.org/10.1007/s12551-016-0247-1.

11. A. G. McArthur and G. D. Wright, "Bioinformatics of Antimicrobial Resistance in the Age of Molecular Epidemiology," *Current Opinion in Microbiology* 27 (2015): 45–50, https://doi.org/10.1016/j.mib.2015.07.004.

12. D. Barh, S. Tiwari, N. Jain, et al., "In Silico Subtractive Genomics for Target Identification in Human Bacterial Pathogens," *Drug Development Research* 72, no. 2 (2010): 162–177, https://doi.org/10.1002/ddr.20413.

13. N. Ünlü, A. Özgen, and C. Aksu CANBAY, "Production and Characterization of Polyvinyl Alcohol Films Containing Essential Oil," *Journal of Biomaterials Science, Polymer Edition* 35, no. 10 (2024): 1537–1549, https://doi.org/10.1080/09205063.2024.2338642.

14. C. A. Canbay and N. Ünlü, "Production and Characterization of Shape Memory Polymeric Nanocomposite Materials," *Journal of Molecular Structure* 1227 (2021): 129708, https://doi.org/10.1016/j.molstruc.2020.129708.

15. H. Sharma and M. Pathak, "Development of PCL/TiO2 Composite as an Efficient Antibacterial, Anticancer Drug and Biocompatible Properties," *Results in Chemistry* 7 (2024): 101534, https://doi.org/10.1016/j.rechem.2024.101534.

16. Clinical and Laboratory Standards Institute, *Performance Standards for Antimicrobial Susceptibility Testing: Twenty-Second Informational*

Supplement (M100-S22) (Clinical and Laboratory Standards Institute, 2012).

17. H. S. Mansur, C. M. Sadahira, A. N. Souza, and A. A. P. Mansur, "FTIR Spectroscopy Characterization of Poly (Vinyl Alcohol) Hydrogel With Different Hydrolysis Degree and Chemically Crosslinked With Glutaraldehyde," *Materials Science and Engineering: C* 28, no. 4 (2008): 539–548, https://doi.org/10.1016/j.msec.2007.10.088.

18. K. Choo, Y. Ching, C. Chuah, S. Julai, and N.-S. Liou, "Preparation and Characterization of Polyvinyl Alcohol-Chitosan Composite Films Reinforced With Cellulose Nanofiber," *Materials* 9, no. 8 (2016): 644, https://doi.org/10.3390/ma9080644.

19. H. Kaur, S. Singh, S. Rode, et al., "Fabrication and Characterization of Polyvinyl Alcohol-Chitosan Composite Nanofibers for Carboxylesterase Immobilization to Enhance the Stability of the Enzyme," *Scientific Reports* 14, no. 1 (2024): 19615, https://doi.org/10.1038/s41598-024-67913-x.

20. F. Bakkali, S. Averbeck, D. Averbeck, and M. Idaomar, "Biological Effects of Essential Oils – A Review," *Food and Chemical Toxicology* 46, no. 2 (2008): 446–475, https://doi.org/10.1016/j.fct.2007.09.106.

21. N. Park, M. A. Friest, and L. Liu, "Enhancing the Properties of Polyvinyl Alcohol Films by Blending With Corn Stover-Derived Cellulose Nanocrystals and Beeswax," *Polymers* 15, no. 21 (2023): 4321, https://doi.org/10.3390/polym15214321.

22. K. Dai, S. Cao, J. Yuan, et al., "Recent Advances of Sustainable UV Shielding Materials: Mechanisms and Applications," *Applied Materials and Interfaces* 17, no. 21 (2025): 30402–30422, https://doi.org/10.1021/acsami.5c04539.

23. A. Alahmad, I. Alghoraibi, R. Zein, et al., "Identification of Major Constituents of *Hypericum perforatum* L. Extracts in Syria by Development of a Rapid, Simple, and Reproducible HPLC-ESI-Q-TOF MS Analysis and Their Antioxidant Activities," *ACS Omega* 7, no. 16 (2022): 13475–13493, https://doi.org/10.1021/acsomega.1c06335.

24. L. Atarés and A. Chiralt, "Essential Oils as Additives in Biodegradable Films and Coatings for Active Food Packaging," *Trends in Food Science and Technology* 48 (2016): 51–62, https://doi.org/10.1016/j.tifs.2015.12.001.

25. S. Roy, R. Ramakrishnan, G. Goksen, S. Singh, and Ł. Łopusiewicz, "Recent Progress on UV-Light Barrier Food Packaging Films—A Systematic Review," *Innovative Food Science and Emerging Technologies* 91 (2024): 103550, https://doi.org/10.1016/j.ifset.2023.103550.

26. T. Hatakeyema, A. Yamauchi, and H. Hatakeyema, "Studies on Bound Water in Poly(Vinyl Alcohol). Hydrogel by DSC and FT-NMR," *European Polymer Journal* 20, no. 1 (1984): 61–64, https://doi.org/10.1016/0014-3057(84)90223-4.

27. R. R. Khasbiullin, Y. V. Kostina, T. F. Petrova, et al., "Residual Water in Polyvinyl Alcohol," *Polymer Science, Series A* 56, no. 5 (2014): 569–578, https://doi.org/10.1134/s0965545x14050095.

28. M. G. A. Vieira, M. A. da Silva, L. O. dos Santos, and M. M. Beppu, "Natural-Based Plasticizers and Biopolymer Films: A Review," *European Polymer Journal* 47, no. 3 (2011): 254–263, https://doi.org/10.1016/j.eurpolymj.2010.12.011.

29. R. Sothornvit and J. M. Krochta, "Plasticizers in Edible Films and Coatings," in *Innovations in Food Packaging* (Elsevier, 2005), 403–433, https://doi.org/10.1016/b978-012311632-1/50055-3.

30. T. M. C. Maria, R. A. de Carvalho, P. J. A. Sobral, A. M. B. Q. Habitante, and J. Solorza-Feria, "The Effect of the Degree of Hydrolysis of the PVA and the Plasticizer Concentration on the Color, Opacity, and Thermal and Mechanical Properties of Films Based on PVA and Gelatin Blends," *Journal of Food Engineering* 87, no. 2 (2008): 191–199, https://doi.org/10.1016/j.jfoodeng.2007.11.026.

31. T. V. Panova, A. A. Efimova, A. K. Berkovich, and A. V. Efimov, "Plasticity Control of Poly(Vinyl Alcohol)–graphene Oxide Nanocomposites," *RSC Advances* 10, no. 40 (2020): 24027–24036, https://doi.org/10.1039/d0ra04150e.

32. N. A. Peppas and E. W. Merrill, "Poly(Vinyl Alcohol) Hydrogels: Reinforcement of Radiation-Crosslinked Networks by Crystallization," *Journal of Polymer Science, Polymer Chemistry Edition* 14, no. 2 (1976): 441–457, https://doi.org/10.1002/pol.1976.170140215.

33. J.-W. Rhim, K. A. Mohanty, S. P. Singh, and P. K. W. Ng, "Preparation and Properties of Biodegradable Multilayer Films Based on Soy Protein Isolate and Poly(Lactide)," *Industrial and Engineering Chemistry Research* 45, no. 9 (2006): 3059–3066, https://doi.org/10.1021/ie051207+.

34. L. Sánchez-González, M. Cháfer, M. Hernández, A. Chiralt, and C. González-Martínez, "Antimicrobial Activity of Polysaccharide Films Containing Essential Oils," *Food Control* 22, no. 8 (2011): 1302–1310, https://doi.org/10.1016/j.foodcont.2011.02.004.

35. D. Ratna and J. Karger-Kocsis, "Recent Advances in Shape Memory Polymers and Composites: A Review," *Journal of Materials Science* 43, no. 1 (2008): 254–269, https://doi.org/10.1007/s10853-007-2176-7.

36. M. Behl and A. Lendlein, "Shape-Memory Polymers," *Materials Today* 10, no. 4 (2007): 20–28, https://doi.org/10.1016/s1369-7021(07)70047-0.

37. Q. Zhao, H. J. Qi, and T. Xie, "Recent Progress in Shape Memory Polymer: New Behavior, Enabling Materials, and Mechanistic Understanding," *Progress in Polymer Science* 49 (2015): 79–120, https://doi.org/10.1016/j.progpolymsci.2015.04.001.

38. Y. Liu, H. Du, L. Liu, and J. Leng, "Shape Memory Polymers and Their Composites in Aerospace Applications: A Review," *Smart Materials and Structures* 23 (2014): 023001, https://doi.org/10.1088/0964-1726/23/2/023001.

39. N. Severino, C. Reyes, Y. Fernandez, et al., "Bacterial Foodborne Diseases in Central America and the Caribbean: A Systematic Review," *Microbiology Research* 16, no. 4 (2025): 78, https://doi.org/10.3390/microbiolres16040078.

40. A. L. Speer, T. C. Grikscheit, J. S. Upperman, and H. R. Ford, "Sepsis and Related Considerations," in *Pediatric Surgery* (Elsevier, 2012), 141–163, https://doi.org/10.1016/b978-0-323-07255-7.00010-6.

41. B. B. Finlay and S. Falkow, "Common Themes in Microbial Pathogenicity Revisited," *Microbiology and Molecular Biology Reviews* 61, no. 2 (1997): 136–169, https://doi.org/10.1128/mmbr.61.2.136-169.1997.

42. B. R. Otto, R. Sijbrandi, J. Luirink, et al., "Crystal Structure of Hemoglobin Protease, a Heme Binding Autotransporter Protein From Pathogenic *Escherichia coli*," *Journal of Biological Chemistry* 280, no. 17 (2005): 17339–17345, https://doi.org/10.1074/jbc.m412885200.

43. O. Sherlock, M. A. Schembri, A. Reisner, and P. Klemm, "Novel Roles for the AIDA Adhesin From Diarrheagenic*escherichia coli*: Cell Aggregation and Biofilm Formation," *Journal of Bacteriology* 186, no. 23 (2004): 8058–8065, https://doi.org/10.1128/jb.186.23.8058-8065.2004.

44. M.-E. Charbonneau, V. Girard, A. Nikolakakis, et al., "O-Linked Glycosylation Ensures the Normal Conformation of the Autotransporter Adhesin Involved in Diffuse Adherence," *Journal of Bacteriology* 189, no. 24 (2007): 8880–8889, https://doi.org/10.1128/jb.00969-07.

45. O. Marchès, T. N. Ledger, M. Boury, et al., "Enteropathogenic and Enterohaemorrhagic *Escherichia coli* Deliver a Novel Effector Called Cif, Which Blocks Cell Cycle G2/M Transition," *Molecular Microbiology* 50, no. 5 (2003): 1553–1567, https://doi.org/10.1046/j.1365-2958.2003.03821.x.

46. N. Bragagnolo, C. Rodriguez, N. Samari-Kermani, et al., "Protein Dynamics in F-Like Bacterial Conjugation," *Biomedicine* 8, no. 9 (2020): 362, https://doi.org/10.3390/biomedicines8090362.

47. J. Moreno, H. Nielsen, O. Winther, and F. Teufel, "Predicting the Subcellular Location of Prokaryotic Proteins With DeepLocPro," *Bioinformatics* 40, no. 12 (2024): 362, https://doi.org/10.1093/bioinformatics/btae677.

48. O. Trott and A. J. Olson, "AutoDock Vina: Improving the Speed and Accuracy of Docking With a New Scoring Function, Efficient Optimization, and Multithreading," *Journal of Computational Chemistry* 31, no. 2 (2010): 455–461, https://doi.org/10.1002/jcc.21334.

49. G. M. Morris, R. Huey, W. Lindstrom, et al., "AutoDock4 and AutoDockTools4: Automated Docking With Selective Receptor Flexibility," *Journal of Computational Chemistry* 30, no. 16 (2009): 2785–2791, https://doi.org/10.1002/jcc.21256.

50. X.-Y. Meng, H.-X. Zhang, M. Mezei, and M. Cui, "Molecular Docking: A Powerful Approach for Structure-Based Drug Discovery," *Current Computer-Aided Drug Design* 7, no. 2 (2011): 146–157, https://doi.org/10.2174/157340911795677602.